Structure, microstructure and determination of optical constants from transmittance data of co-doped $Zn_{0.90}Co_{0.05}M_{0.05}O$ (M=Al, Cu, Cd, Na) films

S. Roguai [a], A. Djelloul [a,*], Corinne Nouveau [b], T. Souier [c], A.A. Dakhel [d], M. Bououdina [d]

[a] *LASPI^2 A Laboratoire des Structures, Propriétés et Interactions Inter Atomiques, Université Abbes Laghrour, Khenchela 40000, Algeria*
[b] *LaBoMaP Laboratoire Bourguignon des Matériaux et Procédés, Arts et Métiers ParisTech of Cluny Campus, F-71250 Cluny, France*
[c] *Masdar Institute of Science and Technology, Material Science and Engineering, PO Box 54224, Abu Dhabi, United Arab Emirates*
[d] *Department of Physics, College of Science, University of Bahrain, PO Box 32038, Bahrain*

ARTICLE INFO

Article history:
Received 25 November 2013
Received in revised form 13 February 2014
Accepted 15 February 2014
Available online 24 February 2014

Keywords:
Thin films
Microstructure
Optical properties
Scanning electron microscopy SEM
X-ray diffraction

ABSTRACT

ZnO, $Zn_{0.95}Co_{0.05}O$ and $Zn_{0.90}Co_{0.05}M_{0.05}O$ (M=Al, Cd, Na, Cu) single phase films have been successfully synthesized by ultrasonic spray pyrolysis technique. Structural analysis by X-ray diffraction show that all the films have hexagonal wurtzite structure with an average crystallite size in the range of 19–25 nm. SEM analysis revealed that Cd and Na preserve the shape of nanopetals observed with ZnO or Co—ZnO films, while the doping with Al or Cu promote the formation of dense films constituted of nanorods. By the application of Levenberg–Marquardt least square method, the experimental transmittance data were fitted perfectly with the transmittance data calculated via a combination of Wemple–DiDomenico model, absorption coefficient of an electronic transition and Tauc–Urbach model. The concentration of absorbing centres N_{Co} and oscillator strength f of d–d transition of Co^{2+} ions are calculated from Smakula's formula.

1. Introduction

Zinc oxide based semiconductors showed a great interest in recent years because of their wide range applications, in particular in the field of spintronics. ZnO is a semiconductor with a large band-gap (E_g = 3.31 eV), large exciton binding energy ~60 meV at room temperature [1] and a transmittance of approximately 0.9 in the visible region. ZnO crystallizes in a wurtzite structure which can be defined by a hexagonal lattice in which the Zn^{2+} ions occupy the tetrahedral sites formed by the O^{2-} ions.

Recently, transition metal-doped semiconductors have been the focus of numerous research investigations because of their unusual optical properties and promising potential for application in opto-electronic devices [2–5]. Among these semiconductors, ZnO that is doped with a small amount of transition metal ions, in particular Co-doped ZnO system has been highly investigated.

Dietl et al. [6] theoretically predicted room temperature ferromagnetism on transition metal (TM) doped ZnO known as diluted magnetic semiconductors (DMS). Since then, investigation of TM-doped ZnO, especially Co-doped ZnO, has attracted considerable attention due to their unique properties. Various deposition techniques have been used for the preparation of Co-doped ZnO thin films [7–10].

It is important to note that the defect environment can be altered when a dopant atom M (Co, Al, Cd, Cu and Na) substitutes a Zn atom. Therefore, it is worth investigating the doping effect on optical properties of ZnO: M system.

The refractive index dispersion plays an important role in optical communication and designing of the optical devices. The knowledge of accurate values of the wavelength dependent complex refractive index of thin films is very important, both from a fundamental and a technological viewpoint. It yields fundamental information on the optical energy band-gap, defect levels, phonon and plasma frequencies, etc.

Numerous theoretical methods have been developed for the determination of the refractive index of thin films. The combination of a normal incidence transmission measurement and a near-normal incidence reflectance measurement has been used for the determination of the refractive index (n) and the extinction coefficient (k) [11–13].

* Corresponding author. Address: Laboratoire des Structures, Propriétés et Interactions Inter Atomiques (LASPI^{2}A), Faculté des Sciences et Technologies, Université Abbes Laghrour, Khenchela 40000, Algeria. Fax: +213 32 33 19 60.
E-mail address: djelloulabdelkader@yahoo.fr (A. Djelloul).

The problem of estimating the thickness and the optical constants of thin films using experimental transmittance data is very challenging from mathematical point of view, as well as has a technological importance. Optical transmittance provides accurate and rapid information on the spectral range where the material transforms from complete opacity to some degree of transparency.

In this work, of ZnO, $Zn_{0.95}Co_{0.05}O$ and $Zn_{0.90}Co_{0.05}M_{0.05}O$ (with M=Al, Cd, Na and Cu) thin films are deposited by ultrasonic spray pyrolysis (USP) technique. The effects of the nature of the co-doping element M on structure, microstructure and optical properties are discussed. A particular attention is given to the theoretical methods used for the determination of the dispersion parameters of the films using only a single transmission spectrum.

2. Experimental part

ZnO, $Zn_{0.95}Co_{0.05}O$ and $Zn_{0.90}Co_{0.05}M_{0.05}O$ (with M=Al, Cd, Na and Cu) films used in this study were prepared by ultrasonic spray pyrolysis. This technique has many advantages, such as better stoichiometry control, better homogeneity, low processing temperature, lower cost, easier preparation of large area films, possibility of using high-purity starting materials, and having an easy coating process of large substrates. The solution used for the investigated films has the following composition: 0.01 M of zinc acetate [$Zn(CH_3COO)_2{\cdot}2H_2O$)] (Fulka 99.9%); 50 ml deionised water (resistivity = 18.2 MΩ cm); 20 ml CH_3OH (Merck 99.5%); and 30 ml C_2H_5OH (Merck 99.5%). Cobalt nitrate hexahydrate 5% (Co, at.%) [$Co(NO_3)_2{\cdot}6H_2O$], copper acetate 5% (Cu, at.%) [$Cu(CH_3COO)_2{\cdot}H_2O$], cadmium acetate 5% (Cd, at.%) [$Cd(CH_3COO)_2{\cdot}2H_2O$], aluminium nitrate hexahydrate 5% (Al, at.%) [$Al(NO_3)_3{\cdot}6H_2O$] and sodium chloride 5% (Na, at.%) [NaCl] has been used as the Co, Cu, Cd, Al and Na source. A small amount of acetic acid was added to the aqueous solution for adjusting the pH value to about 4.8, in order to prevent the formation of hydroxides. Water is the most convenient oxidizing agent. Methanol and ethanol were the obvious choice because of their volatility and thus facilitating quick transformation of the precursor mist into vapor form, which is an important criterion for obtaining good quality films. The ultrasonic spraying system used in this work consists of a commercial ultrasonic atomizer VCX 134 AT and a substrate holder with heater. The ultrasonic vibrator frequency was 40 kHz and the power used was 130 W. The median drop size at 40 kHz is 45 μm. The nozzle–substrate distance was 5 cm and during the deposition, the solution flow rate was held constant at 0.1 ml/min. Further details are reported elsewhere [14,15]. Thin films were deposited onto microscope cover glass substrates ($30 \times 10 \times 1.2\ mm^3$) at the temperature of 450 °C and the deposition time was fixed at 30 and 45 min. The substrate temperature was monitored with a thermocouple and controlled electronically.

X-ray diffraction patterns were recorded using high resolution Rigaku Ultima IV powder X-ray diffractometer equipped with Cu Kα radiation (λ = 1.5418 Å). The film morphology was examined using a (Quanta™ 250 FEG-SEM from FEI company) scanning electron microscope. The transmittances of thin films were measured using a Perkin Elmer UV–VIS–NIR Lambda 19 spectrophotometer in the 190–1800 nm spectral range.

3. Results and discussion

3.1. Structure and microstructure analysis

X-ray diffraction patterns of as-prepared pure ZnO, 5% Co-doped ZnO and co-doped $Zn_{0.90}Co_{0.05}M_{0.05}O$ with M=Na, Al, Cu, and Cd system (Figs. 1a and 1b) reveal the formation of pure single wurtzite phase as confirmed with JCPDS Card No. 00-036-1451. The intensity of diffraction peaks varies considerably and non-homogeneously, depending on the nature (its atomic number) of the doping element and its real concentration within the film after deposition (which will be discussed in SEM/EDX section).

A preferred orientation along (002) direction for all compositions is observed, but the degree of grains orientation along this direction is dependent as well on the nature of the doping element. This was associated with the value of the surface free energy, which might be minimum for ZnO (002) plane during growth process [16].

Qualitative and quantitative phase analyses were carried out using PDXL program. Both lattice parameters (a and c) and microstructural parameters (crystallite size and microstrain) were refined, the results are reported in Table 1. The value of fit

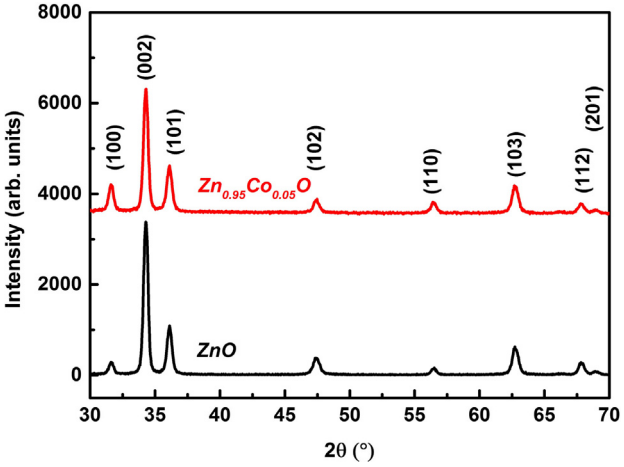

Fig. 1a. XRD patterns of pure ZnO and Co-doped ZnO films.

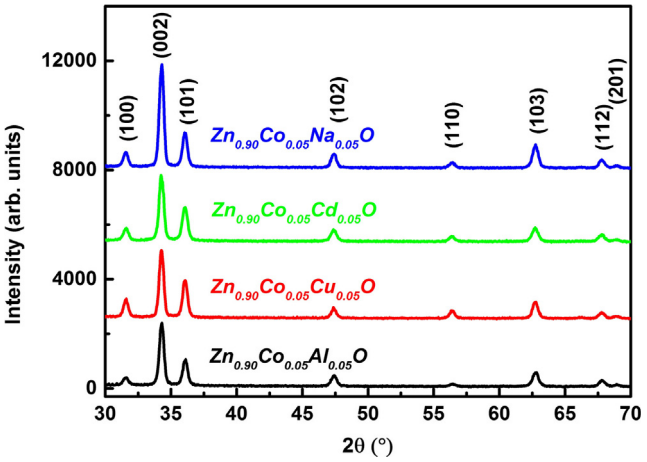

Fig. 1b. XRD patterns of $Zn_{0.90}Co_{0.05}M_{0.05}O$ (M=Na, Al, Cu, and Cd) films.

parameters (Rwp (%) weighted profile R-factor; Rp (%) profile R-factor; Re (%) expected R-factor; S = Rwp/Re and $\chi^2 = S^2$ goodness of fit) indicate a good fit; see Fig. 2 for $Zn_{0.95}Co_{0.05}O$ composition.

Rietveld refinements confirm the formation of single pure ZnO phase with hexagonal ($P6_3mc$) wurtzite type structure for all compositions. The values of lattice parameters of pure ZnO thin film are smaller compared to the values reported in the literature; a = 3.2542 Å and c = 5.2129 Å compared to a = 3.2328 Å and c = 5.1952 Å for ZnO thin film of 357 nm thickness deposited on glass substrate by spray pyrolysis using zinc acetate dehydrate ($Zn(CH_3COO)_2{\cdot}2H_2O$) [17]. This might be caused by the low quality of X-ray diffraction pattern, as the peak shape profile is not well defined. Moreover, it is important to mention that recording an XRD pattern of thin film in powder mode as well as the film thickness, may cause some shift of peaks' position, leading to unreal value of the lattice parameters. In our case, the measurements were carried out using thin film mode, where the height of the sample is optimized before recording the X-ray diffraction pattern. Additionally, Chen et al. [18] reported that both crystallite size and lattice parameter of ZnO film grown on Si (1 1 1) by pulsed laser deposition (PLD) increase with increasing temperature.

After 5% of Co doping, the lattice parameters increase to reach a = 3.2572 Å and c = 5.2162 Å, which is surprising, as the ionic radius of Co^{2+} is smaller than that of Zn^{2+}; 0.079 nm compared to 0.088 nm, respectively. Such discrepancy may be attributed to some Zn^{2+} deficiency when substituted with Co^{2+} and/or oxygen

Table 1
X-ray diffraction Rietveld refinements results.

Composition	Crystallite size (nm)	Microstrain (%)	Lattice parameters (Å)	Rwp (%)	Refinements Rp (%)	Factors Re (%)	S	χ^2
ZnO	25	0.266	3.2542 (5) 5.2129 (7)	16.87	11.84	8.93	1.71	2.92
$Zn_{0.95}Co_{0.05}O$	23	0.289	3.2572 (4) 5.2162 (7)	9.58	7.41	7.63	1.25	1.57
$Zn_{0.90}Co_{0.05}Na_{0.05}O$	23	0.163	3.2603 (4) 5.2145 (6)	10.12	7.57	7.22	1.40	1.96
$Zn_{0.90}Co_{0.05}Al_{0.05}O$	21	0.212	3.2571 (6) 5.2114 (9)	12.71	9.23	8.16	1.56	2.42
$Zn_{0.90}Co_{0.05}Cu_{0.05}O$	22	0.126	3.2592 (3) 5.2148 (5)	9.02	6.83	7.89	1.14	1.30
$Zn_{0.90}Co_{0.05}Cd_{0.05}O$	19	0.194	3.2601 (5) 5.2160 (8)	11.01	8.67	7.67	1.43	2.06

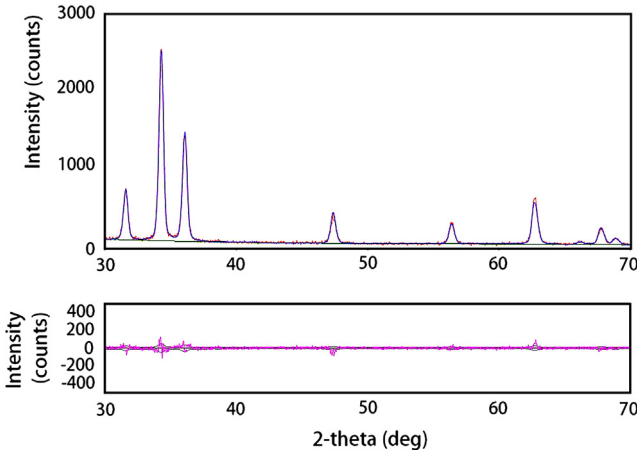

Fig. 2. Rietveld refinements of $Zn_{0.95}Co_{0.05}O$ composition. Solid blue curve: calculated pattern; red solid line: experimental data; solid orange line (down): intensity difference. (For interpretation of the references to colour in this figure legend, the reader is referred to the web version of this article.)

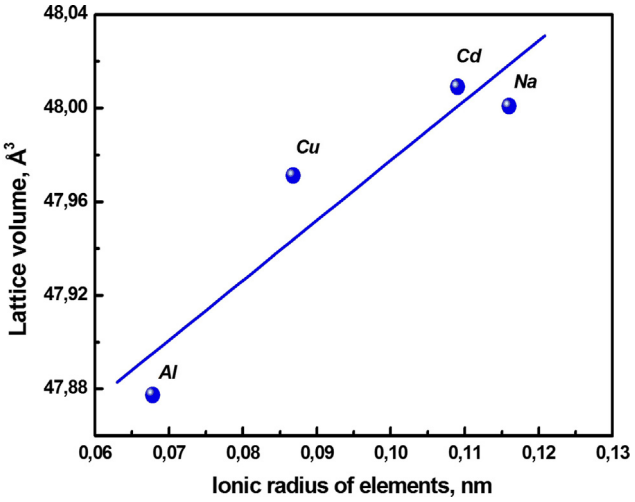

Fig. 3. Evolution of lattice volume ($V = a^2\, c\, \sin 60°$) with the variation of ionic radius of the elements.

stoichiometry (vacancies). Li et al. [19] reported that the lattice parameters of ZnO film deposited on glass substrate by using magnetron sputtering and further annealing in vacuum and oxygen atmosphere decrease, which was attributed to the variation of oxygen vacancy concentration.

Also, some references reported that stress occurring during film deposition may be responsible for the variation of lattice parameter [20], in this case 0.266% for pure ZnO and 0.289% for $Zn_{0.95}Co_{0.05}O$.

The obtained values in this study are slightly smaller than the values $a = 3.2521$ Å and $c = 5.2078$ Å of ZnO powder synthesized by an auto-combustion method [21]. The values for Co-doped ZnO are higher than that of pure ZnO, which are similar to our results.

Moreover, it is observed that the variation of lattice parameters after codoping is in agreement with the change of the ionic radius of the substituting element ($r[Co^{2+}] = 0.079$ nm; and $r[Cu^{2+}] = 0.087$ nm; $r[Na^{+}] = 0.116$ nm; $r[Al^{3+}] = 0.068$ nm; and $r[Cd^{2+}] = 0.109$ nm) by occupying Zn^{2+} ($r = 0.088$ nm) sites within ZnO crystal lattice. The variation of lattice volume with the ionic radius of the doping element shows a linear behaviour, see Fig. 3.

The crystallite size seems to not being affected by the nature and the ionic radius of the doping element (M=Na, Al, Cu and Cd), the average value is around 20 nm. However, the value of microstrain varies considerably with M, which can be attributed to its valence and ionic radius.

Images of the surface of the films were obtained using Secondary Electron (SE) detector and Backscatter Electron detector (BSE). An example of high resolution SEM scans is reported in Fig. 4. To study the effect of the co-dopant type, SEM images were compared to those recorded on pure ZnO (Fig. 4e) and Co-doped ZnO (Fig. 4f).

The doping with Co seems to preserve the ZnO microstructure characterized by the presence of nanopetals emerging perpendicularly to the film surface. One can notice a slight effect of Co-doping on reducing the size and length of nanopetals which is in good agreements with the reduction of crystallite size observed by XRD data. For these two films, the nanopetals have a thickness of 20 nm and a length (or size) of 200–350 nm. In addition to that, a population of nanosized spherical features with a size of 30–60 nm can be observed.

However, it is noticed that additional co-doping of Co—ZnO has a strong effect on the morphology of the film surface. On one hand, Cd and Na preserve the aforementioned nanostructure of Co—ZnO films but characterized with an increase in the size (length) of nanopetals up to 500–800 nm, while their thickness remains almost unaffected. On the other hand, Cu and Al change the morphology of the films. In particular, Al co-doping leads to the formation of dense film showing small grains with a diameter in the range 15–45 nm. A high magnified image of Al—Co ZnO films reveals that these uniform nano-grains are in fact nanorods (or nanowire) grown mainly in the perpendicular direction of the film surface. Few nanorods can be seen also growing horizontally to the film surface. These nanorods can be seen dispersed in smaller quantity and higher size for Na and Cd doped films. It is noted also that the nanorods and even some nanopetals exhibit a hexagonal-like cross-section, implying the occurrence of the wurtzite ZnO crystal structure.

The SEM is equipped with Genesis Energy-dispersive X-ray (EDX) spectroscopy system that was used to determine the chemical composition of the films. An example of EDX spectra of Cu/Co co-doped ZnO film is shown in Fig. 5. In particular, EDX data are analyzed in order to reveal the co-doping effectiveness as well as to check the stoichiometry of the as-prepared oxide films, the results are reported in Table 2. Cu doped films are found to induce the best co-doping of ZnO where the composition of the film is close to the expected one $Zn_{0.9}Co_{0.05}Cu_{0.05}O$. The other films show

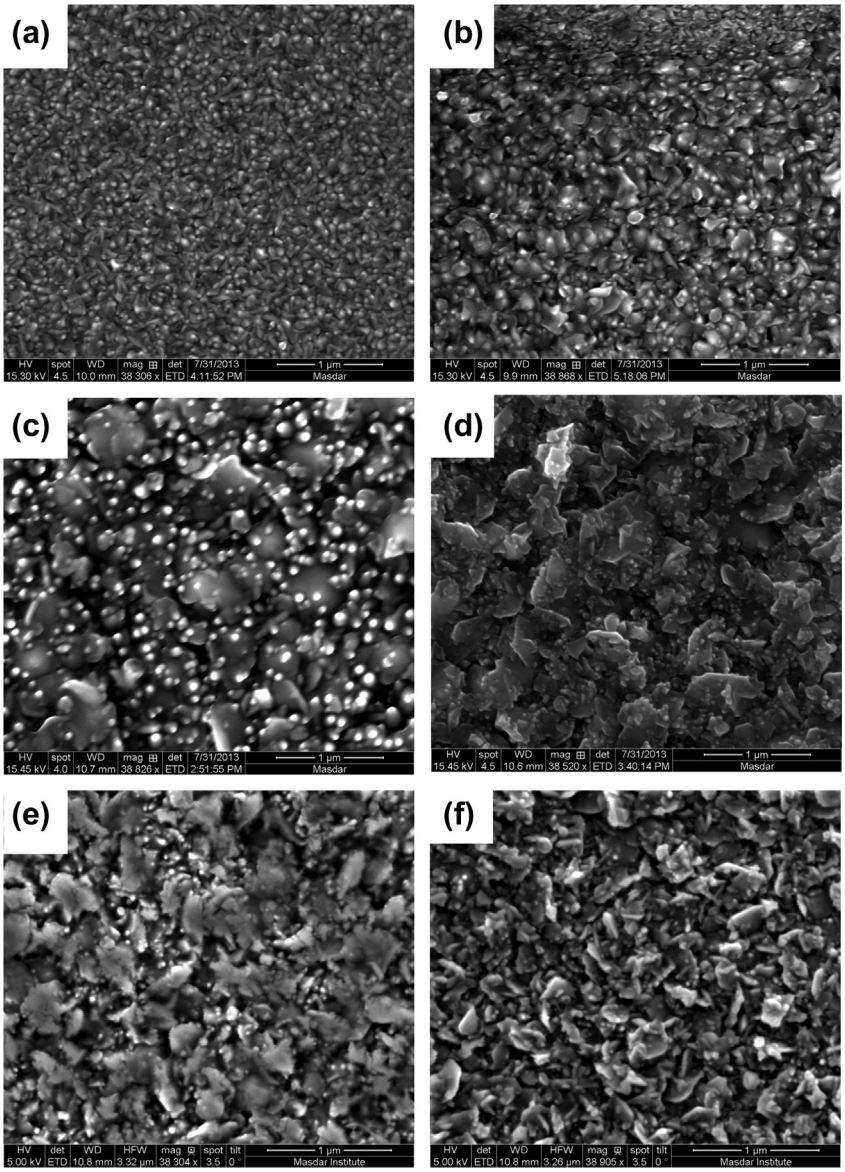

Fig. 4. SEM images of co-doped $Zn_{0.9}Co_{0.05}$ (M) $_{0.05}O$ thin films doped with (a) Al, (b) Cu, (c) Na and (d) Cd. We shows as well (e) pure ZnO and (f) doped $Zn_{0.95}Co_{0.05}O$ thin films.

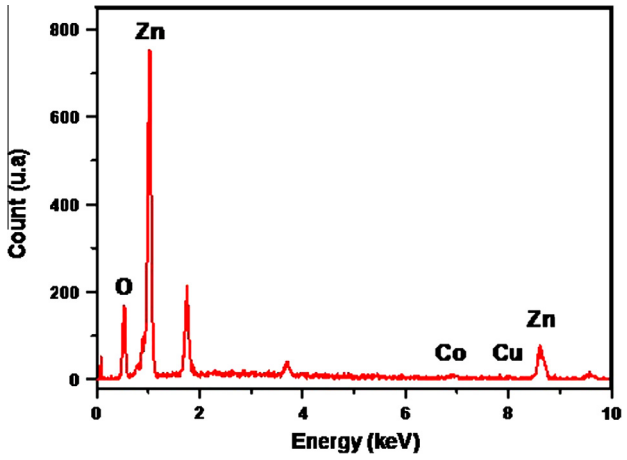

Fig. 5. Example of EDX spectra of co-doped $Zn_{0.9}Co_{0.05}$ $Cu_{0.05}O$ used for composition calculation (see Table 2).

Table 2
Composition and stoichiometry of the thin films obtained by statistical analysis of EDX spectrum.

Co-doping $Zn_{0.9}Co_{0.05}M_{0.05}O$	Zn (at.%)	Co (at.%)	M (at.%)	x (Co)	y (M)
M=Al	40.7	1.8	1.4	0.04	0.03
M=Cu	44.6	2.75	2.6	0.055	0.05
M=Cd	60.3	0.77	3.4	0.01	0.05
M=Na	47.6	3.75	0	0.07	0

a shift from the stoichiometry with the typical atomic composition of $Zn_{0.93}Co_{0.04}Al_{0.03}O$ and $Zn_{0.94}Co_{0.01}Cd_{0.05}O$ are observed for Al and Cd doping respectively. The co-doping with Na was found to be not effective as no trace of this element was evidenced by EDX analysis; the formed film seems to contain Co dopant only.

3.2. Optical properties

The refractive index dispersion plays an important role in optical communication and designing optical devices. Therefore, it is

Table 3
Dispersion parameters for ZnO [22]. Wurtzite (N_C = 4, Z_a = 2, N_e = 8).

Crystal	E_0 (eV)	E_d (eV)	M_{-1}	M_{-3}, 10^{-2} $(eV)^{-2}$	n_∞	n at 598 nm	β (eV)
ZnO	6.4	17.1	2.672	6.523	1.916	1.996	0.27

important to determine dispersion parameters of the films. In the transparent region (extinction coefficient $k = 0$), the dispersion parameters of the films were evaluated using a single-effective-oscillator fit, proposed by Wemple and DiDomenico [22], of the form $n^2 - 1 = E_d E_0/(E_0^2 - E^2)$ where $E = hc/\lambda$ is the photon energy, E_0 the single oscillator energy, and E_d is the dispersion energy. The parameter E_d, which is a measure of the strength of inter-band optical transitions, is found to obey the simple empirical relationship $E_d = \beta N_C Z_a N_e$ where N_C is the coordination number of the cation nearest neighbour to the anion, Z_a is the formal chemical valence of the anion, N_e is the effective number of valence electrons per anion (usually N_e = 8), and for ionic $\beta_i = 0.26 \pm 0.04$ eV. The values of E_0, E_d and β of ZnO are listed in Table 3.

The refractive index dispersion data below the band-gap can be analyzed by the following dispersion relation:

$$n^2 - 1 = \frac{S_0 \lambda_0^2}{1 - (\lambda_0/\lambda)^2} \tag{1}$$

where λ is the wavelength of incident light, S_0 is the average oscillator strength of the absorption band with resonance wavelength λ_0, which is an average oscillator wavelength. Eq. (1) also can be converted as:

$$n^2 - 1 = \frac{(n_\infty^2 - 1)\lambda^2}{\lambda^2 - \lambda_0^2} \tag{2}$$

where n_∞ and λ_0 are the high-frequency refractive index and average oscillator wavelength, respectively.

When absorption bands in the visible and near infrared regions coexist (extinction coefficient, $k \neq 0$), the refractive index dispersion data can be analyzed by the following dispersion relation:

$$n^2 - 1 - k^2 = \frac{(n_\infty^2 - 1)\lambda^2}{\lambda^2 - \lambda_0^2} \tag{3}$$

In the cases where absorbance of a chemical system reveals a band of absorption of a "simple form", an electronic transition is able to correctly describe the same band. A simple Gaussian profile centred on the vertical transition in question is then used to reproduce the structure of this absorption band. This assumes a vertical electronic transition between a state S_i and a state S_j, electron transition wavelength $\lambda_{i\to j}$ and oscillator strength $f_{i\to j}$. The expression of the resulting spectral band $\alpha_{i\to j}$ is proportional to a Gaussian function such as:

$$\alpha_{i\to j}(\lambda) \propto \frac{f_{i\to j}}{\xi'\sqrt{\pi}} \exp\left(-\frac{(\lambda - \lambda_{i\to j})^2}{\xi'^2}\right), \quad \xi' = \frac{\xi}{2\sqrt{\ln(2)}} \tag{4}$$

where ξ represents the width at half maximum of the Gaussian function, or bandwidth. This parameter is chosen empirically by comparison with experiment.

In a simple solid consisting of a host lattice and an impurity ion, the absorption coefficient α for the solid solution can be considered as the sum $\alpha = \alpha_h + \alpha_i$, where α_h, is the absorption from the host lattice and α_i is the contribution to the absorption coefficient from the impurity ion. For ZnO:Co, α_h is equivalent to the absorption coefficient for the un-doped ZnO. The extinction coefficient k is related to the absorption coefficient α by the expression $4\pi k/\lambda$.

The extinction coefficient k in the transparent region ($\lambda \geqslant \lambda_g$) is:

$$k = k_0 \frac{(\exp(B\lambda_g/\lambda) - 1)}{(\exp(B) - 1)} + \frac{\lambda}{4\pi}\left[\alpha_0 + \sum_{j=1}^{q} \alpha_{i\to j}(\lambda)\right] \tag{5}$$

where λ_g – wavelength of absorption region ($E_g(eV) = 1239.8/\lambda_g$ (nm)), i – ground state, j – excited state and q is the number of excited states.

The extinction coefficient k in the region of interband transitions ($\lambda \leqslant \lambda_g$) is:

$$k = k_1\left(1 - \frac{\lambda}{\lambda_g}\right)^r + k_0 \tag{6}$$

where k_0, k_1, B, λ_g, $f_{i\to j}$, ξ' and $\lambda_{i\to j}$ are the fitting parameters and r can have values as 1/2, 3/2, 2, and 3 depending on the nature of the interband electronic transitions, such as direct allowed, direct forbidden, indirect allowed, and indirect forbidden transitions, respectively [23,24]. For ZnO, the value of r is always 1/2, i.e., the fundamental absorption corresponds to allowed direct transition.

In order to calculate the optical constants from the data, one requires formulae which relate the measured values of $T(\lambda)$ and thickness, d, to the real and imaginary components of the refractive index, $N = n\text{-}ik$, for an absorbing film on a transparent substrate. The common approach is to consider the reflection and transmission of light at the three interfaces of the air/film/substrate/air multilayer structure and express the results in terms of Fresnel coefficients.

The system is surrounded by air with refractive index $n_0 = 1$. Taking all the multiple reflections at the three interfaces into account, it can be shown that in the case where $k^2 \ll n^2$, the expression of the transmittance $T(\lambda)$ for normal incidence is given by [25–27]:

$$T = \frac{A\chi}{B - C\chi + D\chi^2} \tag{7}$$

where,

$$A = 16\gamma^2 n_s(n^2 + k^2)$$

$$B = [(n+1)^2 + k^2]\,[(n+1)\,(n + n_S^2) + k^2]$$

$$C = 2\eta[(n^2 - 1 + k^2)(n^2 - n_S^2 + k^2) - 2k^2(n_S^2 + 1)]\cos\varphi - 2k\beta,[2(n^2 - n_S^2 + k^2) + (n_S^2 + 1)(n^2 - 1 + k^2)]\sin\varphi$$

$$D = \eta^2[(n-1)^2 + k^2]\,[(n-1)\,(n - n_S^2) + k^2]$$

$$\varphi = 4\pi nd/\lambda$$

$$\chi = \exp(-\alpha d)$$

$$\alpha = 4\pi k/\lambda$$

$$\gamma = \exp[-\frac{1}{2}(2\pi\sigma/\lambda)^2(1-n)^2] \quad \eta = \exp[-2(2\pi\sigma/\lambda)^2]$$

where σ is the rms height of surface irregularity.

The parameters n and k are the real and imaginary parts of the thin film refractive index, d is the film thickness and n_S is the real substrate refractive index. Knowing the refractive index of the

substrate and putting the values of n and k as computed from Eqs. (3), (5) and (6) into Eq. (7), the theoretical transmittance value, referred to as T_{theo}, can be obtained. Then by the application of Levenberg–Marquardt least square method, the experimental transmittance data (T_{expt}) were fitted completely with the transmittance data calculated (T_{theo}) by Eq. (7) via a combination of Wemple–DiDomenico model, absorption coefficient of an electronic transition and Tauc–Urbach model.

Minimizing a sum of squares ($|T_{expt}-T_{theo}|$) generated for different values of the thickness (d) and wavelength of gap (λ_g) by iterative technique, and finding the corresponding n and k, the exact film thickness and energy band-gap can be calculated.The refractive-index of glass substrate, taken from Ref. [28] is:

$$n_S^2 = 1 + \frac{1.0396\times\lambda^2}{\lambda^2 - 6.0069\times10^3} + \frac{0.23179\times\lambda^2}{\lambda^2 - 2.0017\times10^4} + \frac{1.0104\times\lambda^2}{\lambda^2 - 1.0356\times10^8} \quad (8)$$

Transmittance spectra were taken at room temperature to study the optical properties of ZnO, $Zn_{0.95}Co_{0.05}O$ and $Zn_{0.90}Co_{0.05}M_{0.05}O$ films. The transmittance spectra of all films show the characteristic Co^{2+} absorptions in the visible and near infrared spectral region at the wavelengths of 565, 611, 657, 1297, 1410 and 1648 nm. The first three peaks are the predominant absorptions.

For Al^{3+}, Cu^{2+}, Cd^{2+} and Na^{+} codoped $Zn_{0.95}Co_{0.05}O$ films, similar absorption pattern is observed as in $Zn_{0.95}Co_{0.05}O$, but the absorption is more pronounced in codoped systems.

The dopant ion (Co^{2+}) transforms the colourless host lattice (ZnO) into green. If the concentration of the dopant ion is low, the interaction between the dopant ions can be neglected. This is what was considered here as an isolated absorbing centre. The real distance between two Zn atoms in the studied systems is about ~0.326 nm, while the Zn atoms in $Zn_{0.95}Co_{0.05}O$ are present in tetrahedral structures with Zn—O distances of 0.196 nm. For uniformly distributed Co ions, the mean distance between Co ions that have been substituted into Zn sites within ZnO crystal lattice can be estimated via [29] $N_{at} = (4/3)(Z/V_C)\,\pi\, r^3$, where r is the average radius of an atomic sphere and N_{at} is the number of atoms in the sphere. The structural parameters for $Zn_{0.95}Co_{0.05}O$ are: $a = 0.32572$ nm, $c = 0.52162$ nm; volume of unit cell (V_C) = 47.92×10^{-3} nm^3; $Z = 2$. For zinc atoms in a wurtzite structure of $Zn_{0.95}$ $Co_{0.05}O$, $Z/V_C = 41.73$ nm^{-3}. In $Zn_{0.95}Co_{0.05}O$ film, 5% of zinc sites are occupied by Co ions. Therefore, the 20th zinc site from the probe atom is occupied by cobalt. Using the above calculation, the average distance between Co ions is estimated to be around ~0.48 nm, which means that the nearest Co ion to a probe Co ion is located in the next unit cell.

According to the ligand field theory [30], splitting of $3d^7$ (Co^{2+}) orbital should result in the spectroscopic terms $^4A_2$ (A: no degeneracy), $^4T_2$, $^4T_1$ (T: three fold degeneracy), and ^2E (E: two fold degeneracy). For Co^{2+} in ZnO crystal lattice, Co^{2+} substitutes for some Zn^{2+}, and adopts tetrahedral ligand coordination. The 3d levels are extremely host sensitive. The strong crystal field in ZnO leads to the splitting of 3d electron orbits of Co^{2+} and produces the ground level: $^4A_2$, and the excited states: ^2E, $^4T_2$, and $^4T_1$, etc. The transitions from $^4A_2$ to $^4T_2$, and $^4T_1$ are spin-allowed.

Figs. 6 and 7 show UV spectra of ZnO, $Zn_{0.95}Co_{0.05}O$ and $Zn_{0.90}Co_{0.05}M_{0.05}O$ films. The absorption peaks located at 657, 610, and 567 nm for $Zn_{0.95}Co_{0.05}O$ and $Zn_{0.90}Co_{0.05}M_{0.05}O$ films can be assigned as $^4A_2(F) \rightarrow {}^2E(G)$, $^4A_2(F) \rightarrow {}^4T_1(P)$, and $^4A_2(F) \rightarrow {}^2A_1$ (G), of Co^{2+}, attributed to the crystal field transitions in the high spin state of Co^{2+} in the tetrahedral coordination, suggesting that the tetrahedrally coordinated Co^{2+} ions substitute for Zn^{2+} ions in the hexagonal ZnO wurtzite structure [31]. Between 1272 and 1647 nm, additional crystal field transition was observed, namely $^4A_2(F) \rightarrow {}^4T_1(F)$ transition.

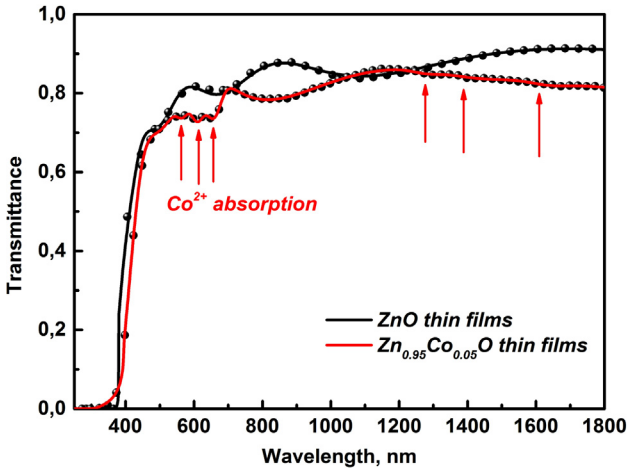

Fig. 6. Transmission spectrum of $Zn_{0.95}Co_{0.05}O$ films deposited on glass substrate at 450 °C. Transmission spectrum of ZnO film prepared at the same condition is presented as a reference. Measured (full circles) and calculated (solid lines) transmittance spectra of films.

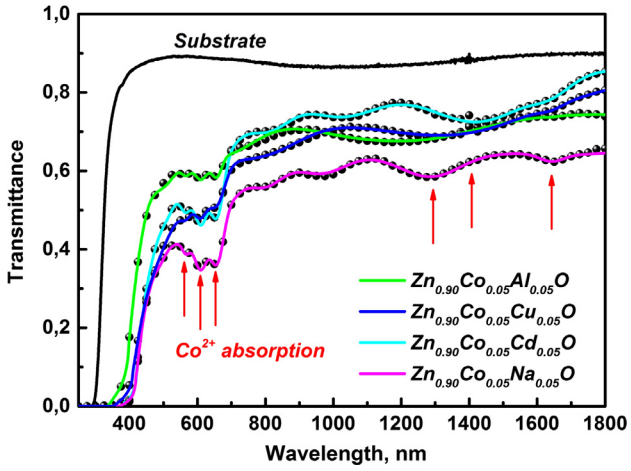

Fig. 7. Transmission spectra of $Zn_{0.90}Co_{0.05}M_{0.05}O$ (with M=Al, Cd, Na and Cu) films deposited on glass substrate at 450 °C. Transmittance of the bare glass substrate, $T_{Sbstrate}$, is also shown. Measured (full circles) and calculated (solid lines) transmittance spectra of films.

The solid curve in Figs. 6 and 7 corresponds to the curve fitting using Eq. (7) and the symbol represents the experimental data. The Figures reveal a reasonable good fitting to the experimental data, implying the accurate determination of the parameters of Eq. (7). The values of d, E_g, E_d, E_0, rms and n_∞, extracted by fitting the experimental data with Eq. (7) are listed in Table 4.

The optical energy band-gap of pure ZnO film was estimated as 3.26 eV. This value is slightly smaller than the bulk value of 3.31 eV [1] and in good agreement with previously reported data of ZnO thin films [32]. Table 5 shows some results for comparison [32–34].

An obvious red shift of the absorption edges can be observed in $Zn_{0.95}Co_{0.05}O$ and co-doped $Zn_{0.90}Co_{0.05}M_{0.05}O$ with M=Na, Al, Cu, and Cd films. The value of the direct optical band-gap is reduced from 3.26 to 2.94 eV. The s-d and p-d exchange interactions lead to a negative and positive correction to the conduction band and the valence band edges, resulting into band-gap narrowing. The interaction leads to corrections in the energy bands; the conduction band is lowered while the valence band is raised thereby causing the band-gap to shrink [35,36]. The decrease of energy

Table 4
Dispersion parameters of the films extracted by fitting the experimental data with Eq. (7).

	Thickness (nm)	E_g (eV)	E_d (eV)	E_0 (eV)	n at 598 nm	n_∞	M_{-1}	M_{-3}, $\times 10^{-2}$ (eV)$^{-2}$	σ (nm)
ZnO	486	3.258	11.334	6.018	1.771	1.698	1.883	5.200	38
$Zn_{0.95}Co_{0.05}O$	341	3.140	12.151	5.793	1.845	1.760	2.097	5.770	8
$Zn_{0.90}Co_{0.05}Al_{0.05}O$	484	3.106	11.110	5.713	1.800	1.716	1.945	5.958	43
$Zn_{0.90}Co_{0.05}Cu_{0.05}O$	568	3.026	11.237	5.590	1.825	1.735	2.010	6.433	76
$Zn_{0.90}Co_{0.05}Na_{0.05}O$	1283	2.956	10.031	5.535	1.763	1.677	1.812	5.915	73
$Zn_{0.90}Co_{0.05}Cd_{0.05}O$	1071	2.946	10.106	5.535	1.767	1.681	1.826	5.960	76

Table 5
Some results of ZnO films deposited by spray pyrolysis technique.

	Crystallite size (nm)	Band-gap (eV)	Thickness (nm)	Refractive index
Roguai et al.	25	3.26	486	1.77
[32]	20	3.26	240	1.76
[33]	26	3.28	259	1.88
[34]	15	3.29	325	1.72

value from 3.26 eV (pure ZnO) to 3.14 eV ($Zn_{0.95}Co_{0.05}O$) appears to originate from active transitions involving 3d levels in Co^{2+} ions and strong sp–d exchange interactions between the itinerant 'sp' carriers (band electrons) and the localized 'd' electrons of the dopant [37–39]. This red shift of band-gap E_g with the incorporation of Co^{2+} into ZnO has already been reported by several researchers [40–42]. Al^{3+}, Cu^{2+}, Na^+ and Cd^{2+} codoping of $Zn_{0.95}Co_{0.05}O$ result in decreasing the value of E_g from 3.14 to 3.10 eV, 3.04 eV, 2.95 eV and 2.94 eV, respectively. The shrinking of the band-gap due to Al^{3+}, Cu^{2+}, Na^+ and Cd^{2+} codoping is consistent with the general trend previously observed by other authors [43–46].

Using single oscillator energy (E_0) and dispersion energy (E_d) obtained from the fitted transmittance spectra reported in Table 4, M_{-1} and M_{-3} moments of the optical spectra can be determined from the following two equations [16]:

$$E_0^2 = \frac{M_{-1}}{M_{-3}} \tag{9}$$

$$E_d^2 = \frac{M_{-1}^3}{M_{-3}} \tag{10}$$

These moments represent the measure of the average bond strength. The two moments M_{-1} and M_{-3} were calculated from the data of E_0 and E_d and are given in Table 4. It can be noticed that the values of M_{-1} and M_{-3} change with the nature of the doping element. Comparing the results in Table 4 with the absorption coefficient in the near infrared spectral region, it can be concluded that M_{-3} increases with the incorporation of cobalt in the host lattice.

The refractive index of ZnO film versus wavelength is calculated, as shown in Fig. 8, and is found to be lower than that of bulk ZnO [16]. But for both cases, the relationship between the refractive index and the wavelength exhibits the same tendency.

The calculated refractive indices of ZnO, $Zn_{0.95}Co_{0.05}O$ and $Zn_{0.90}Co_{0.05}M_{0.05}O$ (with M=Al, Cd, Na and Cu) films (Figs. 8 and 9) exhibit a function of the wavelength. It is found that the refractive indices at

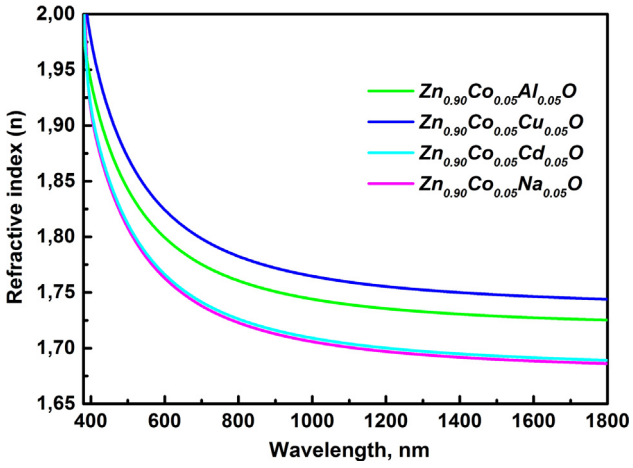

Fig. 9. Refractive index of $Zn_{0.90}Co_{0.05}M_{0.05}O$ (with M=Al, Cd, Na and Cu) films deposited on glass substrate at 450 °C.

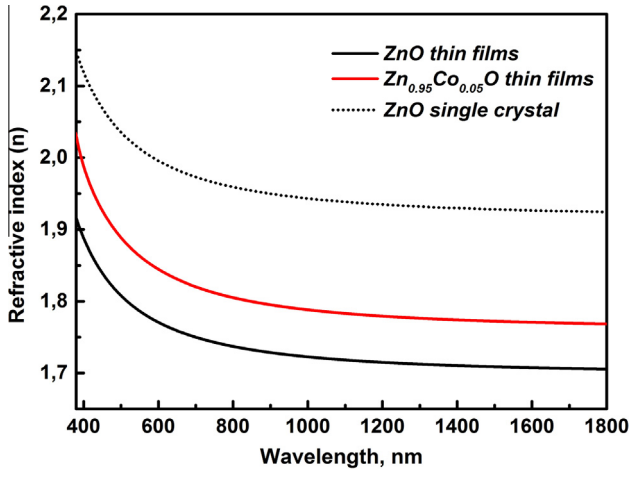

Fig. 8. Refractive index of $Zn_{0.95}Co_{0.05}O$ grown on glass substrate at T_S = 450 °C. Refractive index of ZnO film prepared at the same condition is presented as a reference.

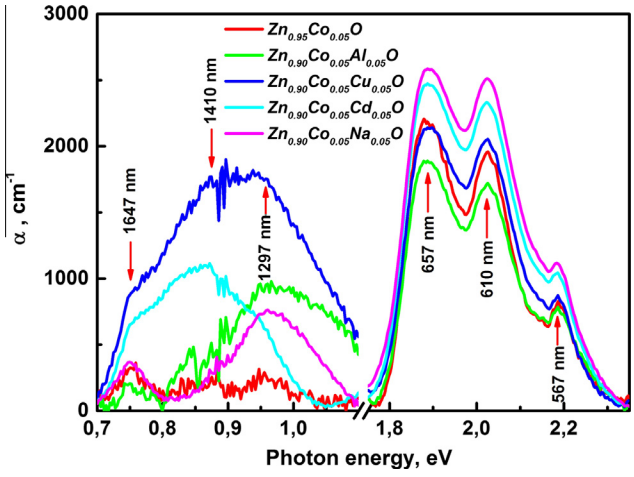

Fig. 10a. The absorption coefficient versus photon energy of $Zn_{0.95}Co_{0.05}O$ and $Zn_{0.90}Co_{0.05}M_{0.05}O$ (with M=Al, Cd, Na and Cu) films deposited on glass substrate at 450 °C.

598 nm of ZnO, $Zn_{0.95}Co_{0.05}O$ and $Zn_{0.90}Co_{0.05}Cu_{0.05}O$ films are equal to 1.77, 1.84 and 1.82, respectively.It can be noticed that the above calculated refractive indices are equal or a little greater than that of ZnO film prepared under the same conditions. This might be due to the fact that the index of refraction is sensitive to structural defects (for example voids, dopants, inclusions), thus it can provide an important information concerning the microstructure of the material. Gases like CH_3COOH, H_2O, etc. were produced as $Zn(CH_3COO)_2$ was oxidized into ZnO. Consequently, pores can be easily formed due to the release of these gases. The porosity P is calculated from optical constants using the Lorentz–Lorenz equation [47]:

$$P = 1 - \frac{(n_{film}^2 - 1)(n_{bulk}^2 + 2)}{(n_{film}^2 + 2)(n_{bulk}^2 - 1)} \tag{11}$$

where the value of n_{film} (1.771 at 598 nm) represents the refractive indices of porous ZnO films and n_{bulk} represents the refractive indices of ZnO bulk which is 1.996 at same wavelength. The average mass density of the film ρ_{film} is related to the porosity (P) and bulk density (ρ_{bulk}) of ZnO through Eq. (12):

$$\rho_{film} = \rho_{bulk}(1 - P) \tag{12}$$

We determined $P = 0.1659$ and $\rho_{film} = 4.68$ g cm^{-3} against the bulk density $\rho_{bulk} = 5.61$ g cm^{-3}. The concentration of cobalt cations N_{Co} for 5 at.% doping level in the films can be calculated as:

$$N_{Co} = \frac{\rho_{film} N_{Av}}{M} \times 0.05 \tag{13}$$

where N_{Av} is the Avogadro constant and M the molar mass. With the values $\rho_{film} = 4.68$ g cm^{-3}, $N_{Av} = 6.022 \times 10^{23}$ mol^{-1}, and molar mass for ZnO, $M = 81.408$ g mol^{-1}, the calculated value of N_{Co} is 1.73×10^{21} cm^{-3}.

The oscillator strength is often used as a method for calculating the concentration of impurities in a host from known f values and measured absorption coefficients. Classically, the oscillator strength f represents the number of electric dipole oscillators that can be simulated by the radiation field (in the dielectric dipole approximation) and has a value close to one for strongly allowed transitions. The integrated absorption of an optical transition is related to the concentration of absorbing centres N, index of refraction n, and oscillator strength f by the well-known Smakula formula [48]:

$$Nf = 8.21 \times 10^{16}\ \text{cm}^{-3} \frac{n}{(n^2 + 2)^2} \int \alpha(E)\, dE \tag{14}$$

where n is the refractive index of intersubband transitions, α is the decadic absorption coefficient in cm^{-1} and E is the energy in eV. For Gaussian absorption bands the integral is:

$$\frac{1}{2}\sqrt{\frac{\pi}{\ln 2}}\alpha_{\max} W \tag{15}$$

with maximum absorption α and full width at half maximum W. Eq. (14) can be expressed as follow:

$$Nf = 8.74 \times 10^{16}\ \text{cm}^{-3} \frac{n}{(n^2 + 2)^2} \alpha_{\max} W \tag{16}$$

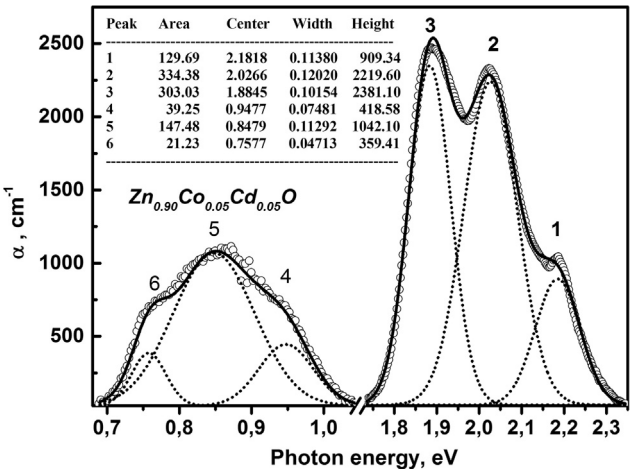

Fig. 10b. The Gaussian deconvolution of the absorption coefficient of $Zn_{0.90}Co_{0.05}Cd_{0.05}O$ films deposited on glass substrate at 450 °C.

Table 6
Concentration of absorbing centres N and oscillator strength f of d–d transition of Co^{2+} ions. 1: 567 nm ($^4A_2(F) \rightarrow {}^2E(G)$); 2: 610 nm ($^4A_2(F) \rightarrow {}^4T_1(P)$); 3: 657 nm ($^4A_2(F) \rightarrow {}^2A_1(G)$); 4: 1297 nm ($^4A_2(F) \rightarrow {}^4T_1(F)$); 5: 1410 nm ($^4A_2(F) \rightarrow {}^4T_1(F)$); 6: 1647 nm ($^4A_2(F) \rightarrow {}^4T_1(F)$).

	1	2	3	4	5	6
$Zn_{0.95}Co_{0.05}O$: $d = 341$ nm, $N_{Co} = 4.332 \times 10^{20}$ cm^{-3}, $\Sigma f_{i\rightarrow j} = 0.065$						
Refractive index	1.857	1.842	1.831	1.777	1.774	1.770
$f_{i\rightarrow j}$, $\times 10^{-3}$	6.839	18.419	18.740	2.728	9.369	9.369
N, $\times 10^{20}$ cm^{-3}	0.490	0.639	0.556	2.282	0.080	0.285
$Zn_{0.90}Co_{0.05}Al_{0.05}O$: $d = 484$ nm, $N_{Co} = 6.8 \times 10^{20}$ cm^{-3}, $\Sigma f_{i\rightarrow j} = 0.043$						
Refractive index	1.811	1.796	1.784	1.732	1.730	1.727
$f_{i\rightarrow j}$, $\times 10^{-3}$	3.821	11.997	6.339	21.049	/	0.208
N, $\times 10^{20}$ cm^{-3}	1.102	0.918	1.530	0.309	/	2.941
$Zn_{0.90}Co_{0.05}Cu_{0.05}O$: $d = 568$ nm, $N_{Co} = 5.420 \times 10^{20}$ cm^{-3}, $\Sigma f_{i\rightarrow j} = 0.225$						
Refractive index	1.836	1.821	1.808	1.752	1.748	1.746
$f_{i\rightarrow j}$, $\times 10^{-3}$	2.588	7.677	13.292	193	7.656	1.671
N, $\times 10^{20}$ cm^{-3}	1.167	1.802	0.740	0.052	0.938	0.721
$Zn_{0.90}Co_{0.05}Na_{0.05}O$: $d = 1283$ nm, $N_{Co} = 5.694 \times 10^{20}$ cm^{-3}, $\Sigma f_{i\rightarrow j} = 0.043$						
Refractive index	1.775	1.759	1.747	1.694	1.691	1.688
$f_{i\rightarrow j}$, $\times 10^{-3}$	3.117	11.551	11.629	7.063	7.599	2.071
N, $\times 10^{20}$ cm^{-3}	1.784	1.502	1.146	0.726	0.096	0.440
$Zn_{0.90}Co_{0.05}Cd_{0.05}O$: $d = 1071$ nm, $N_{Co} = 4.933 \times 10^{20}$ cm^{-3}, $\Sigma f_{i\rightarrow j} = 0.130$						
Refractive index	1.778	1.762	1.750	1.697	1.695	1.691
$f_{i\rightarrow j}$, $\times 10^{-3}$	3.396	11.327	10.959	82.688	18.714	3.168
N, $\times 10^{20}$ cm^{-3}	1.520	1.466	1.193	0.025	0.409	0.320

It is difficult to quantify the absorbance due to the Co^{2+} d–d transitions since the overall value of the transmittance for each film is different. Therefore, the absorption coefficient ($\alpha \approx (1/d) \times \ln(1/T)$) was used since it is normalized by the film thickness (d) as shown in Fig. 10a. It can be observed that in the near infrared spectral region, the absorption coefficient drastically increases due to co-doping especially when the co-dopant is copper ion. Fig. 10b shows the mathematical treatment of the absorption coefficient. By optimizing the peak position and half-width of the Gaussian peaks, it was possible to obtain a good fit for the multi-peak combination. The Gaussian peaks (dashed lines) are shown at the bottom of Fig. 10b, while the solid line represents the linear combination of the multi-Gaussian peaks with a constant background. The Gaussian peak position, area, width (eV) and height (α_{max}, cm^{-1}) are shown in the inset of Fig. 10b. Mathematical treatment of the absorption coefficient has shown that wide visible and near infrared spectral region consists of a series of overlapping bands. Six dominating bands are characterized by 0.75, ~0.85, ~0.95, ~1.88, ~2.03 and ~2.18 eV.

Knowing the oscillator strengths $f_{i\to j}$ as calculated from Eq. (7), refractive index value of intersubband transitions, i.e. at $\lambda_{i\to j}$ of films, α_{max} and full width at half maximum W as found by Gaussian deconvolution of the absorption coefficient, allows to calculate from Smakula's formula the concentration of absorbing centres N.

The obtained values of the concentration of absorbing centres (N) and oscillator strength (f) of the fingerprint of d–d transitions of Co^{2+} ions situated in the T_d symmetry sites are given in Table 6.

The sum of the oscillator strength ($\Sigma f_{i\to j}$) from ground state $^4A_2(F)$ to all other states varies from 0.04 to 0.22 for the investigated films. The concentration of absorbing centres (Co^{2+}) of d–d transitions increases from 4.3×10^{20} up to 6.8×10^{20} cm^{-3} but less than the calculated value ~1.73×10^{21} cm^{-3}.

As mentioned above, the values of the direct optical band-gap is reduced from 3.26 to 2.94 eV. This significant band-gap reduction is due to enhanced Co^{2+} ions incorporation in the films as well as the co-doping effect as confirmed by the obtained concentration of absorbing centres. Doping with Al^{3+}, Na^{+}, Cd^{2+} and Cu^{2+} ions greatly increases the concentration of absorbing centres and results in enhancing the Co^{2+} incorporation in the films.

4. Conclusion

X-ray diffraction analysis using the Rietveld method shows that the as-deposited ZnO, 5% Co-doped ZnO and co-doped $Zn_{0.90}Co_{0.05}M_{0.05}O$ (M=Na, Al, Cu, and Cd) films are pure single wurtzite phase. The lattice parameters vary linearly with increasing ionic radius of the doping element.

The nature of the co-dopant element is found to influence considerably the film morphology, grain size and stoichiometry of the formed oxides. The doping effectiveness was revealed by EDX analysis of the chemical composition of the films. While the co-doping with Cu appears to be effective and leads to the expected film composition, the co-doping with Na was not successful. The addition of Al and Cd are found to lead to the formation of oxide films with a slight shift of its stoichiometry. The morphology of Cd and Na co-doped films is similar to that of Co—ZnO and ZnO films characterized by the formation of nanopetals, whereas Cu and Al additions change the morphology and lead to the growth of dense films characterised by the presence of nanorods or nanowires.

An optical model, which combines the Wemple–DiDomenico model, absorption coefficient of an electronic transition and Tauc–Urbach model, has been proposed to simulate the optical constants and thicknesses of Co doped ZnO and co-doped $Zn_{0.90}Co_{0.05}M_{0.05}O$ (M=Na, Al, Cu, and Cd) films from normal incidence transmittance. It is found that the simulated transmittance is well consistent with the measured transmittance. The refractive index dispersion curves obey the single oscillator model. The dispersion parameters and optical constants of the films were determined. These parameters changed with Co, Al, Cd, Cu and Na dopants. The concentration of absorbing centres N_{Co} and oscillator strength f of d–d transition of Co^{2+} ions are also calculated from Smakula's formula.

References

[1] S. Oktik, Prog. Cryst. Growth Charact. 17 (1988) 171–240.
[2] H.M. Yang, S. Nie, Mater. Chem. Phys. 114 (2009) 279–282.
[3] M. Yang, Z.X. Guo, K.H. Qiu, J.P. Long, G.F. Yin, D.G. Guan, S.T. Liu, S.J. Zhou, Appl. Surf. Sci. 256 (2010) 4201–4205.
[4] H. Saal, T. Bredow, M. Binnewies, Phys. Chem. Chem. Phys. 11 (2009) 3201–3209.
[5] G.M. Kumar, P. Ilanchezhiyan, J. Kawakita, M. Subramanian, R. Jayavel, Cryst. Eng. Commun. 12 (2010) 1887–1892.
[6] T. Dietl, H. Ohno, F. Matsukura, J. Cibert, D. Ferrand, Science 287 (2000) 1019–1022.
[7] Y.X. Wang, X. Ding, Y. Cheng, Y.J. Zhang, L.L. Yang, H.L. Liu, H.G. Fan, Y. Liu, J.H. Yang, Cryst. Res. Technol. 44 (5) (2009) 517–520.
[8] C. Song, F. Zeng, K.W. Geng, X.B. Wang, Y.X. Shen, F. Pan, J. Magn. Magn. Mater. 309 (2007) 25–30.
[9] A. Zukova, A. Teiserskis, S. van Dijken, Y.K. Gun'ko, V. Kazlauskiene, Appl. Phys. Lett. 89 (2006) 232503–232505.
[10] H. Matsui, H. Tabata, Phys. Rev. B 75 (2007) 014438–014447.
[11] T.C. Paulick, Appl. Opt. 25 (1986) 562–564.
[12] R.D. Bringans, J. Phys. D: Appl. Phys. 10 (1977) 1855–1861.
[13] R.E. Denton, R.D. Campbell, S.G. Tomlin, J. Phys. D: Appl. Phys. 5 (1972) 852–863.
[14] K. Bouzid, A. Djelloul, N. Bouzid, J. Bougdira, Phys. Status Solidi A 206 (2009) 106–115.
[15] A. Djelloul, M.S. Aida, J. Bougdira, J. Lumin. 130 (11) (2010) 2113–2117.
[16] H.S. Lee, J.Y. Lee, T.W. Kim, D.W. Kim, W.J. Cho, J. Mater. Sci. 39 (2004) 3525–3528.
[17] S. Aydogu, O. Sendil, M.B. Coban, Chin. J. Phys. 50 (1) (2012) 89–100.
[18] X.C. Chen, J.P. Zhou, H.Y. Wang, P.S. Xu, G.Q. Pan, Chin. Phys. B 20 (9) (2011) 096102–096104.
[19] X. Li, Y. Wang, W. Liu, G. Jiang, C. Zhu, Mater. Lett. 85 (2012) 25–28.
[20] D. Raoufi, T. Raoufi, Appl. Surf. Sci. 255 (2009) 5812–5817.
[21] G. Pei, C. Xia, F. Wu, J. Xu, J. Alloys Comp. 467 (2009) 539–540.
[22] S.H. Wemple, M. DiDomenico, Phys. Rev. B3 (1971) 1338–1351.
[23] J. Tauc, in: F. Abelès (Ed.), Optical Properties of Solids, North-Holland, Amsterdam, London, 1972, pp. 277–313.
[24] E.A. Davis, N.F. Mott, Phil. Mag. 22 (1970) 903–922.
[25] R. Swanepoel, J. Phys. E. Sci. Instrum. 16 (1983) 1214–1222.
[26] A.K.S. Aqili, A. Maqsood, Appl. Opt. 41 (1) (2002) 218–224.
[27] J. Szczyrbowski, A. Czapla, Thin Solid Films 46 (1977) 127–137.
[28] http://refractiveindex.info/?group=GLASSES&material=BK7.
[29] S.-Y. Seo, C.-H. Kwak, S.-H. Kim, S.-H. Park, I.-J. Lee, S.-W. Han, J. Cryst. Growth 346 (1) (2012) 56–60.
[30] P. Koidl, Phys. Rev. B 15 (5) (1977) 2493–2499.
[31] H.A. Weakliem, J. Chem. Phys. 36 (1962) 2117–2140.
[32] A. Ashour, M.A. Kaid, N.Z. El-Sayed, A.A. Ibrahim, Appl. Surf. Sci. 252 (22) (2006) 7844–7848.
[33] F. Paraguay, W. Estrada, D.R. Acosta, E. Andrade, M.M. Yoshida, Thin Solid Films 350 (1) (1999) 192–202.
[34] T.P. Rao, M.C. Kumar, S.A. Angayarkanni, M. Ashok, J. Alloys Comp. 485 (1) (2009) 413–417.
[35] X. Qiu, L. Li, G. Li, Appl. Phys. Lett. 88 (2006) 114103–114113.
[36] J.I. Pankove, Optical Processes in Semiconductor, Prentice-Hall, New Jersey, 1971.
[37] B. Panigrahy, M. Aslam, D. Bahadur, J. Phys. Chem. C 114 (2010) 11758–11763.
[38] I. Ozerov, F. Chabre, W. Marine, Mater. Sci. Eng. C 25 (2005) 614–617.
[39] P. Lommens, P.F. Smet, C.M. Donega, A. Meijerink, L. Piraux, S. Michotte, S.M. Tempfli, D. Poelman, Z. Hens, J. Lumin. 118 (2006) 245–250.
[40] S. Maensiri, P. Laokul, S. Phokha, J. Magn. Magn. Mater. 305 (2006) 381–387.
[41] A.S. Pereira, A.O. Ankiewicz, W. Gehlhoff, A. Hoffmann, S. Pereira, T. Trindade, M. Jrundmann, M.C. Carmo, N.A. Sobolev, J. Appl. Phys. 103 (2008) 07D140.
[42] M. Ivill, S.J. Pearton, S. Rawal, L. Leu, P. Sadik, R. Das, A.F. Hebard, M. Chisholm, J.D. Budai, D.P. Norton, New J. Phys. 10 (2008) 065002–065017.
[43] Q.H. Li, D.L. Zhu, W.J. Liu, Y. Liu, X.C. Ma, Appl. Surf. Sci. 254 (2008) 2922–2926.
[44] M. Oztas, M. Bedir, Thin Solid Films 516 (2008) 1703–1709.
[45] J. Lv, K. Huang, X. Chen, J. Zhu, C. Cao, X. Song, Z. Sun, Opt. Commun. 284 (12) (2011) 2905–2908.
[46] T. Makino, Y. Segawa, M. Kawasaki, A. Ohtomo, R. Shiroki, K. Tamura, T. Yasuda, H. Koinuma, Appl. Phys. Lett. 78 (2001) 1237–1239.
[47] M.R. Baklanov, K.P. Mogilnikov, V.G. Polovinkin, F.N. Dultsev, J. Vac. Sci. Technol. B 18 (2000) 1385–1391.
[48] A. Smakula, Z. Phys. 59 (1930) 603–614.